UDK 622.337:531/534
Original scientific article/Izvirni znanstveni članek

ISSN 1580-2949
Mater. Tehnol.

RESEARCH ON REFLECTION CRACKING CHARACTERISTICS OF WARM-MIX RECYCLED ASPHALT MORTAR UNDER THE EFFECT OF FREEZE-THAW CYCLES

RAZISKAVE ZNAČILNOSTI ODBOJNEGA POKANJA TOPLE MEŠANICE RECIKLIRANE ASFALTNE MALTE V POGOJIH CIKLIČNEGA SPREMINJANJA TEMPERATURE

Jian Gao[1], Zhiqiang Liu[2], Chao Li[3,*], Lan Wang[3,4], Yudong Ma[5]

[1]Inner Mongolia Transportation Group Mengtong Maintenance Co., Ltd, Hohhot 010051, China
[2]College of Science, Inner Mongolia University of Technology, Hohhot 010051, China
[3]School of Civil Engineering, Inner Mongolia University of Technology, Hohhot 010051, China
[4]Inner Mongolia Key Laboratory of Green Construction and Intelligent Operation and Maintenance of Civil Engineering, Hohhot 010051, China
[5]China Construction Eighth Engineering Division Corp., Ltd Shanghai 200000, China

Prejem rokopisa – received: 2025-01-11; sprejem za objavo – accepted for publication: 2025-05-21

doi:10.17222/mit.2025.1369

The reflection cracking behavior of warm-mix recycled asphalt mortar (WRAM) under freeze-thaw cycles was investigated using a combination of the overlay test and digital image correlation (DIC) technology. Based on the crack images of specimens, the average crack growth rate (*V*) was proposed as an index to characterize the macroscopic reflection cracking behavior of WRAM. Additionally, the correlation between *V* and temperature, salt-solution concentration, and freeze-thaw cycles was analyzed. A meso-index cracking damage factor (D_A) was proposed based on the vertical strain (*Eyy*), considering the effects of the salt-solution concentration and freeze-thaw cycles. The results indicate that with the progression of freeze-thaw cycles, both *V* and D_A of WRAM specimens exhibit an increasing trend, and V increases as the temperature decreases. *V* is an effective index for characterizing the macroscopic reflection cracking behavior of WRAM and is strongly correlated with temperature, salt-solution concentration, and freeze-thaw cycles. D_A effectively reflects the cracking damage due to WRAM reflection cracks after freeze-thaw cycles. *V* and D_A are recommended as comprehensive indices for evaluating the reflective cracking behavior of asphalt mortar from both macro and micro perspectives.

Keywords: warm-mix recycled asphalt mortar, freeze-thaw cycle, reflection cracking characteristics, digital image correlation technology, cracking damage factor

V članku avtorji opisujejo "refleksno" (odbojno) pokanje (angl.: reflection cracking) tople mešanice reciklirane asfaltne mase (WRAM; angl.: warm mix recycled asphalt mortar) v pogojih cikličnega spreminjanja temperature; *zamrznitev-otoplitev* (angl.: freeze-thaw cycles). Raziskavo so izvajali s pomočjo kombinacije dveh metod; i.e.: testa prekrivanja (angl.: Overlay Test) in korelacijske tehnologije digitalnega skeniranja posnetkov (DIC; angl.: Digital Image Correlation Technology). Na osnovi posnetkov razpok na vzorcih so avtorji predlagali vrednosti za povprečno hitrost širjenja razpok *(V)* kot indeks, ki karakterizira makroskopsko refleksno pokanje WRAM. Dodatno so avtorji analizirali in določili povezavo med *V* in temperaturo, koncentracijo soli v raztopini in cikličnim spreminjanjem temperature. Določili so tudi mezo-indeks na osnovi vertikalne deformacije (*Eyy*), ki določa poškodbe zaradi pokanja (D_A), upoštevajoč slanost in ciklično spreminjanje temperature. Rezultati raziskav so pokazali, da s povečevanjem amplitude cikličnega spreminjanja temperature, naraščata tako *V* in D_A preiskovane tople mešanice asfaltne malte. S preizkusi so ugotovil, da se V preizkušancev WRAM zmanjšuje z naraščajočo temperaturo. Indeks *V* je učinkovit pokazatelj velikosti makroskopskega refleksnega pokanja WRAM, ki je močno odvisen od temperature, koncentracije soli v raztopini in cikličnega spreminjanja temperaturea. D_A učinkovito kaže nivo refleksnih poškodb na WRAM po cikličnem spreminjanju temperature. Avtorji v članku poudarjajo, da se indeksa *V* in D_A lahko učinkovito uporablja za evaluacijo oziroma oceno refleksnega pokanja asfaltnih malt, tako na makro kot tudi na mikroskopskem nivoju.

Ključne besede: topla mešanica reciklirane asfaltne malte, ciklično spreminjanje temperature (zamrznitev-otoplitev), značilnosti pokanja, korelacijska tehnologija digitalnega slikanja, faktor poškodbe zaradi refleksnega pokanja

1 INTRODUCTION

The design and technology development of green low-carbon asphalt pavement functional materials oriented toward carbon neutrality is a hot topic of concern in the field of pavement engineering at present. The reclaimed asphalt pavement (RAP) technology, as an advanced, green, and low-carbon regeneration means, has received attention from scholars at home and abroad.[1,2] The plant-mixed hot recycling construction process for asphalt mixtures is common practice. Still, the high temperature in the production of hot-mix reclaimed asphalt mixtures can cause secondary RAP aging, thus affecting road performance.[3] Therefore, warm-mix recycled mixtures are increasingly popular with road workers; it is generally accepted that the warm-mix technology is more beneficial for integrating new and old asphalt in asphalt mixtures.[2,4]

*Corresponding author's e-mail:
lichao@imut.edu.cn (Chao Li)

L. P. Ingrassia et al.[5] monitored the structural properties and stiffness of hot-mix and warm-mix asphalt mixture pavements using in-situ Falling Weight Deflectometer (FWD) tests and laboratory Indirect Tensile Stiffness Modulus (ITSM) tests. It was found that WMA mixtures have higher stiffness and longer service life than HMA mixtures. Asphalt mortar is the base material in asphalt mixtures, and the variation in performance is closely related to the properties of the asphalt mixture. G. Nie et al.[6] tested the shear deformation resistance and high and low temperature performance of asphalt mortars using the rotational viscosity test, cone penetration test, and BBR test. They also evaluated the rutting resistance and low-temperature cracking resistance of asphalt mixtures using the rutting test and small-beam bending test. They found that the performance of asphalt mortars has a decisive role in the road performance of the mixtures using the correlation analysis. At the same time, the repeated action of traffic loads and temperature changes can induce reflection cracking in asphalt pavements. Although initially it does not affect the load-bearing capacity of a pavement structure, continuous infiltration of moisture along the cracks, erosion and alternating cycles of pavement temperature can lead to significant deterioration. Under the constant action of traffic loads, the cracks present in the subgrade may develop stress concentrations and gradually extend toward the surface layer until cracks develop.[7] Especially in seasonal freezing areas, asphalt pavements may undergo several freeze-thaw cycles in a year so that the infiltrated water keeps freezing and melting, further aggravating its damage, thus being an essential factor in pavement performance degradation.[8,9] Therefore, considering the climatic conditions of seasonal freezing areas, it is imperative to study the anti-cracking properties of warm-mix recycled asphalt mortar under freeze-thaw cycles.

Reflective cracks are one of the primary forms of early damage in asphalt pavements. Their formation process is more complex, mainly divided into two stages: crack sprouting and crack expansion.[10] Road workers use relevant indexes to characterize the anti-cracking properties and reveal the reflection cracking mechanism through the Hamburg wheel tracking test, fatigue loading test, three-point bending test, direct tensile cracking test, indirect tensile cracking test, reflection cracking based on motion simulation system, and MMLS3 accelerated loading reflection cracking simulation test.[11–17] However, these test methods have not effectively advanced the study of the anti-reflective cracking ability of asphalt pavements due to issues such as significant discrepancies from actual traffic loads or high test costs.[18]

L. F. Walubita et al.[19–21] investigated the reflection cracking characteristics of HMA pavements using monotonic loading OT tests and noted the promising potential of this test method in evaluating the crack resistance of HMA mixtures. T. M. Phan et al.[22] accurately estimated the anti-reflective cracking ability of WMA-coated fiber, wax-coated fiber, and uncoated fiber asphalt mixtures with OT tests, using the crack expansion rate (Ci). The results showed that the asphalt mixture containing WMA-coated fiber had the best cracking resistance.

In summary, many scholars have researched the reflection cracking phenomenon of asphalt-based materials through various macroscopic testing methods and achieved remarkable results in promoting pavement performance improvement. However, relying only on a single macroscopic approach does not comprehensively describe the anti-reflective cracking ability of asphalt-based materials. Therefore, this study investigated the reflection cracking characteristics of warm-mix recycled asphalt mortar (WRAM) under freeze-thaw cycles using the overlay test (OT) combined with the digital image correlation (DIC) technique. Firstly, the anti-reflective cracking ability of WRAM at different numbers of freeze-thaw cycles was evaluated using the crack progression rate (CPR). Secondly, the average crack expansion rate (V) was used to characterize the expansion of WRAM reflective cracks at different temperatures and freeze-thaw cycles. At the same time, a polynomial equation was constructed for V versus temperature, salt solution concentration, and the number of freeze-thaw cycles. Finally, the cracking damage factor (D_A) was proposed based on the meso-scale vertical strain (Eyy), revealing the reflective cracking resistance of WRAM from the perspective of crack expansion and damage accumulation. Study results provide a reference for the promotion and application of warm-mix regeneration technology in cold regions and a new means to characterize the reflection cracking behavior of asphalt-based materials.

2 EXPERIMENTAL MATERIALS AND DESIGN

2.1 Experimental materials

The base asphalt used in this study was Panjin 90# asphalt. The selection of new aggregates and mineral filler was based on the specifications for the expressways outlined in the Technical Specifications for Construction of Highway Asphalt Pavements (JTG F40-2004) to ensure proper gradation of the asphalt mixture.[23] The new aggregates were basalt with particle sizes of 0–3 mm and 3–5 mm, while the mineral filler was limestone powder. The reclaimed asphalt pavement (RAP) aggregate, composed of basalt with a particle size of 0–5 mm, was collected from the G55 expressway in northern China after ten years of service[24]. The warm-mix agent and regenerating agent used in the test were both SMC-type normal-temperature regenerating agents. The main components included a 3 % dispersant (nonionic surfactant), a 1.75 % titanate coupling agent, and a 1.5 % reinforcing agent (rubber-like polymer). The matrix asphalt and SMC-related technical specifications are shown in **Tables 1** and **2**.

In the preliminary research conducted by our team, warm-mix recycled asphalt mortars with RAP contents of 0, 30, 50, and 70 % were investigated. The asphalt mortar with the 0 % RAP content was prepared using a hot-mix method without the addition of the SMC rejuvenator. Among the tested formulations, the WRAM containing 30 % RAP and 14 % SMC (by mass of old asphalt) exhibited the best overall performance. Therefore, this study focuses on the WRAM with 30 % RAP content, specifically examining the effects of freeze-thaw cycles on its resistance to reflective cracking.[25]

Table 1: Technical specifications of the matrix asphalt

Technical index	Test results	Technical requirements	Test methods
Penetration (25 °C, 100 g, 5 s, 0.1 mm)	93.6	80–100	JTG E20 T 0604
Softening point (°C)	47.6	≥45	JTG E20 T 0606
Ductility (15 °C, cm)	>100	100	JTG E20 T 0605

Table 2: Test results of base indexes for SMC normal-temperature rejuvenating-agent

Test projects	Test results	Technical requirements	Results determination
Appearance	Light yellow jelly shape	Light yellow jelly shape	Conforms to requirements
Density (25 °C, g/cm^3)	0.962	0.85–1.05	Conforms to requirements
100 °C Rotational viscosity (Pa·s)	0.85	≤1.2	Conforms to requirements
Flash point (°C)	155	140–160	Conforms to requirements

Cui Kai et al.[26] determined the mineral composition design and asphalt dosage for asphalt mortar by removing the coarse aggregate from the asphalt mixture and keeping the percentage of fine aggregate sieve residue consistent with the original mix. In this study, the WRAM mineral composition was designed using a method based on the mineral gradation of an AC-20 warm-mix recycled asphalt mixture with 30 % RAP. The final oil-to-sand ratio for 30 % WRAM was set at 6 %. The final results of the WRAM mineral composition design are shown in **Table 3** and **Table 4**.

2.2 Specimen formation

The mixing and compaction temperature of WRAM was 145 °C. In accordance with the OT test procedure (TEX-248-F), cylindrical specimens were formed (150 mm diameter ×170 mm height) using a Superpave Gyratory Compactor. They were then cut into OT test standard specimens (150 × 75 × 38 mm). The specific preparation process and a test specimen are shown in **Figure 1**.

For DIC image acquisition, the surface of the OT standard specimen must be evenly coated with matte white paint as the base layer to enhance the quality of

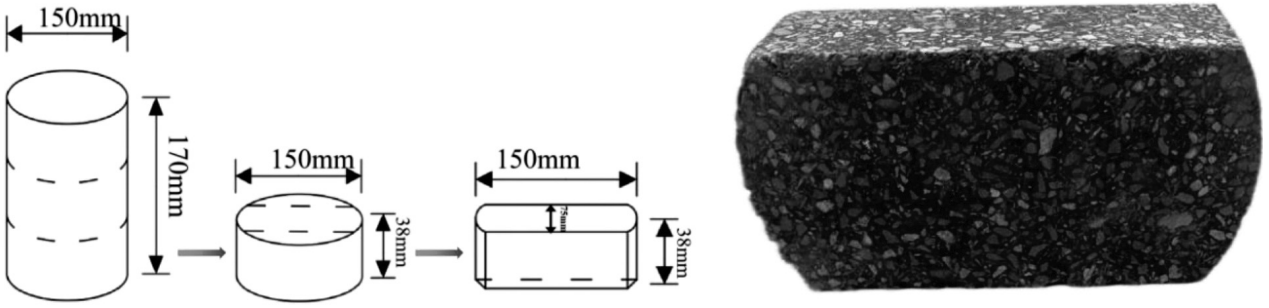

Figure 1: OT specimen preparation and the OT specimen

Table 3: Mineral design gradation of 30 % RAP AC-20 warm-mix recycled asphalt mixture

Grading	Sieve size (mm) and passing rate (%)											
	26.5	19	16	13.2	9.5	4.75	2.36	1.18	0.6	0.3	0.15	0.075
Upper limit of gradation	100	100	92	80	72	56	44	33	24	17	13	7
Lower limit of gradation	100	90	78	62	50	26	16	12	8	5	4	3
Median gradation	100	95	85	71	61	41	30	22.5	16	11	8.5	5
Synthetic gradation	100	100	90.1	68.4	46.5	36.2	28.8	21.9	15.2	10.0	7.3	5.1

Table 4: Mineral composition design of 30 % warm-mix recycled asphalt mortar

Sieve size (mm)	4.75	2.36	1.18	0.6	0.3	0.15	0.075	Mineral powder
WRAM percentage of sieve remainder (%)	17	15.8	15.4	11.9	6.2	5.0	11.7	17
30%-WRAM passing rate (%)	83	67.2	51.8	39.9	33.7	28.7	17	0

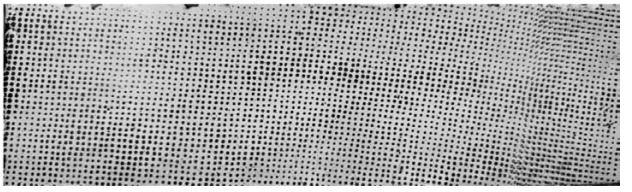

Figure 2: Schematic diagram showing the OT specimen's speckle pattern

surface data capture. Then, a paint roller is used to apply matte black paint on the specimen's surface, creating a random speckle pattern. A schematic diagram illustrating the creation of the OT specimen's random speckle pattern is shown in **Figure 2**.

2.3 Experimental design of the freeze-thaw cycle

In view of the large temperature difference between day and night in northern China, asphalt pavement is susceptible to freeze-thaw damage and high frequency of snowfall in winter. Road workers often use the method of spreading cloth-based de-icing salt to melt snow and ice on the road. To simulate the icing and melting of asphalt pavement in winter, the freeze-thaw cycle test was conducted using indoor high- and low-temperature alternating chambers. Our team found that when the number of freeze-thaw cycles was 20 and the salt concentration was 8 %, the trend of high- and low-temperature performance of the asphalt mixtures was reflected more comprehensively.[27–29] Therefore, in this study, de-icing salt concentrations of 0 % and 8 % were selected, along with freeze-thaw counts of 10 and 20. Before the freeze-thaw cycle test, an OT specimen was immersed in water and 8-% salt solution for saturation. Then, it was kept under a vacuum of 97.3 kPa for 15 min until the normal pressure was restored. The specimen was then removed and placed in a plastic test box containing either water or the salt solution for 1 hour. Finally, the semicircular specimen in the plastic test box containing water or the salt solution was put into a high-and-low temperature cycling chamber. Each freeze-thaw cycle consisted of a –20 °C freeze for 8 hours, and a 60 °C thaw for 16 h. (In this paper, the notation a-b-c refers to a test condition with a °C temperature, b % salt solution concentration, and c freeze-thaw cycles.)

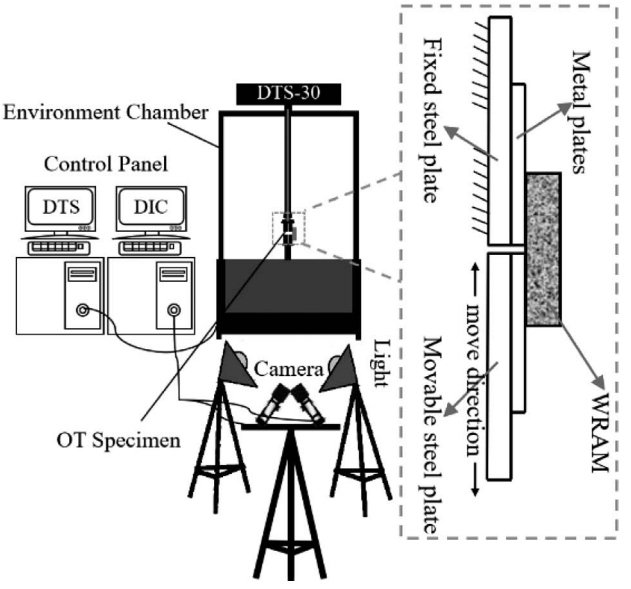

Figure 3: OT test procedure

2.4 DIC-based overlay test experimental design

The overlay test is mainly used to characterize the reflection cracking characteristics of asphalt concrete pavement, so this method was chosen to evaluate the reflection cracking characteristics of WRAM. Before the test, the specimens were attached to a pair of steel plates with gaps, using an appropriate amount of phenolic epoxy resin. Each steel plate was fixed at one end and could be moved horizontally at the other. The spacing between the two plates was 2 mm, as shown in **Figure 3**. The test temperature was 0 °C and 25 °C. The test loading was controlled with triangular waveform displacement. The maximum horizontal tensile displacement was 0.68 mm at 0 °C and 0.9 mm at 25 °C. A test loading cycle took 4 s, 2 s for loading and 2 s for unloading. In this test, in accordance with the OT test procedure (TEX-248-F), the loading cycle count was set to 1000 as the test endpoint.

The DIC method is mainly used to compare the locations and shapes of the scattered speckles on the surface of a specimen before and after deformation. After the specimen deforms, the movement of the speckles in a specific area is tracked and recorded as a digital signal. Finally, Vic-3D image processing software is used to analyze and process the displacement and deformation fields in the horizontal and vertical directions to obtain the deformation information for the specimen surface. In this study, a reflection cracking test was carried out on WRAM using a DTS-30 tester, and the DIC image acquisition system was used for real-time observation. The testing process is illustrated in **Figure 3**.

3 RESULTS AND DISCUSSION

3.1 Analysis of reflection cracking characteristics of warm-mix recycled asphalt mortar

V. Garcia et al.[30] believe that the crack progression rate (CPR) can characterize the flexibility of asphalt materials during the crack propagation process. The larger the CPR value, the faster the crack development and the lower the crack resistance of the material. Therefore, to quantify the impact of freeze-thaw cycling on the anti-reflective cracking characteristics of WRAM, CPR was selected to characterize the reflection cracking characteristics of WRAM at the macro scale. The relationship between the peak load of a specimen and the number of

Table 5: Calculation results for the WRAM crack progression rate

Indicators/Specimens	25-0-0	25-20-10	25-0-20	25-8-10	25-8-20	0-0-0	0-0-10	0-0-20	0-8-10	0-8-20
CPR	0.2897	0.2976	0.3959	0.4134	0.5736	0.3048	0.4271	0.4481	0.4534	0.6603
R^2	0.68	0.62	0.77	0.79	0.71	0.68	0.84	0.91	0.89	0.87

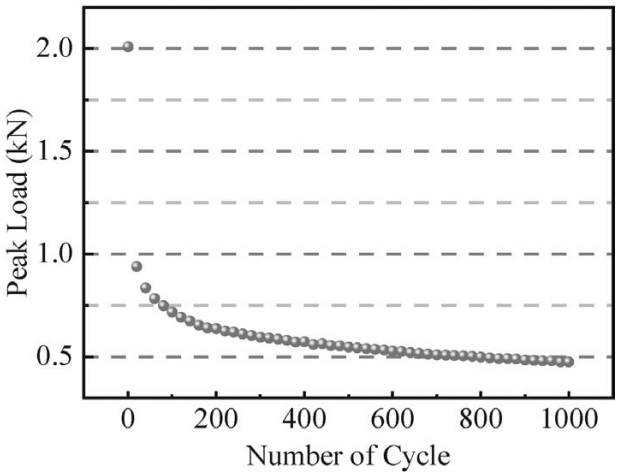

Figure 4: Relationship between the peak load and number of cycles

cycles is given in **Figure 4**. As can be seen, at the beginning of the test loading, the peak load in each cycle drops sharply, and when it drops to a certain degree, cracks appear in the specimen. Then a stable decline phase starts; at this point, the peak load decreases linearly and slowly with the increase in the number of cycles. The CPR is obtained by fitting a normalized peak load-cycle count curve using a power function regression equation, defined as the absolute value of the power exponent. An example of calculation is shown in **Figure 5**.

Table 5 shows the crack progression rate (CPR) for warm-mix recycled asphalt mortar (WRAM) specimens subjected to different freeze-thaw cycles at 25 °C and 0 °C. As can be seen from the table, compared with the original specimens, when the temperature was 25 °C, the CPR of 0–10, 0–20, 8–10, and 8-20 WRAM specimens

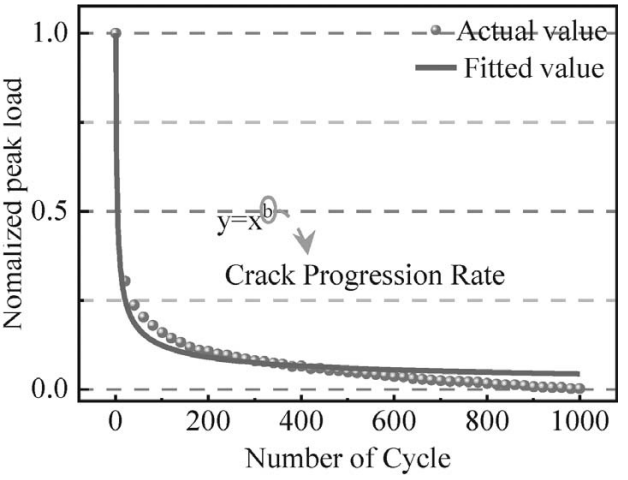

Figure 5: Schematic diagram of the crack progression rate calculation

increased by 2.7, 36.7, 42.7, and 98.0 %, respectively. When the test temperature dropped to 0 °C, the CPR of 0–10, 0–20, 8–10 and 8–20 WRAM specimens increased by 40.1, 47.0, 48.8, and 116.7 %, respectively. This indicates that regardless of the temperature and salt solution concentration, the CPR of the WRAM specimens showed an increasing trend with the increase in the number of freeze-thaw cycles, while the anti-reflective cracking ability of the specimens gradually decreased.

Further analysis revealed that the R^2 values of the CPR fitting results for 0–0, 0–10, 0–20, 8–10, and 8–20 at 25 °C and 0–0 WRAM specimens at 0 °C were small, indicating a weak correlation. This may be attributed to the significant heterogeneity of the asphalt mortar, which makes it difficult to achieve complete internal uniformity during specimen preparation. In addition, the crack propagation behavior in some specimens was unstable during loading. The presence of internal defects rendered the crack propagation paths and rates unpredictable, leading to considerable variability in the test data. Consequently, the coefficient of determination (R^2) was low, indicating a weak correlation. At 0 °C, the CPR showed superiority when evaluating the anti-reflective cracking ability after the WRAM specimens were subjected to stronger freeze-thaw cycles, with R^2 values being greater than 0.8. Therefore, there are limitations to using CPR to investigate the resistance to reflection cracking of WRAM specimens under different freeze-thaw cycling conditions.

The impact of different freeze-thaw cycle conditions on the specimens is inconsistent. The irregularity in the shape of the fine aggregate also leads to significant differences in the length of cracks produced at the end of the test in the WRAM specimens under different freeze-thaw conditions. Therefore, by studying the differences in the crack length (L) of the specimens at the end of the test, we can visually and more accurately elucidate the cracking characteristics of reflected cracks in WRAM specimens under different freeze-thaw conditions. A calculation schematic is shown in **Figure 6**. At the same time, to clarify the crack expansion pattern of WRAM specimens under different freeze-thaw cycles, the average crack expansion rate (V) is also calculated and plotted as a column chart, shown in **Figure 7**. Specific calculation steps of L and V can be divided into 3 steps:

1) A high-speed CCD camera for DIC was used to acquire crack images of the specimens at the end of the test. Meanwhile, approximate locations of the cracks were determined from the images obtained. The cracks were divided into i segments according to the degree of

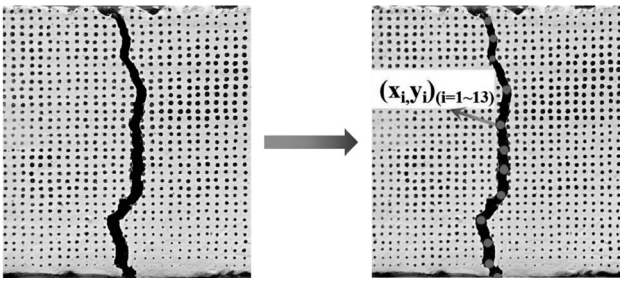

Figure 6: Schematic diagram of crack length calculation

curvature of the cracks, and then the coordinates at the nodes of each segment were obtained using the drawing software and noted as (x_i, y_i). Since the development of a crack was irregular, it was assumed that it was composed of multiple ideal smooth line segments.

2) The coordinates at each small crack node on the specimen surface were recorded and converted using the proportional conversion factor k_1. The critical crack extension length L_i between nodes was calculated and the total crack length L was obtained by summing all L_i values, as shown in Equation (1). The calculation results for L are shown in **Table 6**.

$$L = \sum_{i=1}^{n} k_1 \cdot \sqrt{(x_i - x_{i-1})^2 + (y_i - y_{i-1})^2} \quad (1)$$

3) The V of a specimen can be obtained from the ratio of L to the loading period N, as shown in Equation (2).

$$V = \frac{L}{N} \quad (2)$$

Table 6: Crack length L of WRAM under different freeze-thaw cycles

Freeze-thaw condition	Crack length/mm	Freeze-thaw condition	Crack length/mm
25-0-0	15.58	0-0-0	16.11
25-0-10	19.69	0-0-10	21.01
25-0-20	21.34	0-0-20	22.66
25-8-10	28.71	0-8-10	29.92
25-8-20	32.34	0-8-20	34.21

Figure 7 shows warm-mix recycled asphalt mortar (WRAM) specimens subjected to different freeze-thaw cycles at 25 °C and 0 °C, illustrating how the change in the temperature is reflected in the average crack expansion rate (V). As can be seen from the figure, compared with the original specimens, when the temperature was 25 °C, the V of 0–10, 0–20, 8–10, and 8–20 WRAM specimens increased by 24.6, 36.9, 84, and 107.6 %, respectively; and when the test temperature was 0 °C, the V of 0–10, 0–20, 8–10, and 8–20 WRAM specimens increased by (30.4, 40.7, 85.7 and 112.3) %, respectively. This indicates that, regardless of the temperature and salt solution concentration, with the freeze-thaw cycles increasing, the more severe the freeze-thaw damage of the WRAM specimens, the more significant the V change, and the lower the anti-reflective ability. This is because, during the freezing of a specimen, the decrease in the temperature leads to the contraction of the pores inside the WRAM specimen and its surface, making more aqueous solution being squeezed into the interior of the specimen and condensed into ice, producing a larger frost swelling force. Under the action of the frozen expansion force, tiny cracks appear inside it. During the thawing process, the ice condensed in the pores melts and water enters the microcracks.[31] Eventually, under the effect of constant displacement, the peeling of asphalt and aggregate is intensified, and the anti-reflective cracking ability of the specimen deteriorates.

Further analysis revealed that the V of 0–10, 0–20, 8–10, and 8–20 WRAM specimens increased by (3.2, 6.6, 6.6, 4.2, and 5.9) %, respectively, when the test temperature decreased from 25 °C to 0 °C, indicating that the temperature decrease weakens the anti-reflective cracking ability of WRAM specimens to some extent. This is because WRAM is a temperature-sensitive material. The asphalt gradually hardens during the temperature decrease, weakening the material's deformation capacity and intensifying the generation and expansion of cracks in the specimens.

At the same time, the V growth rate of WRAM specimens after salt freeze-thaw cycles was higher than that after water freeze-thaw cycles, regardless of the tempera-

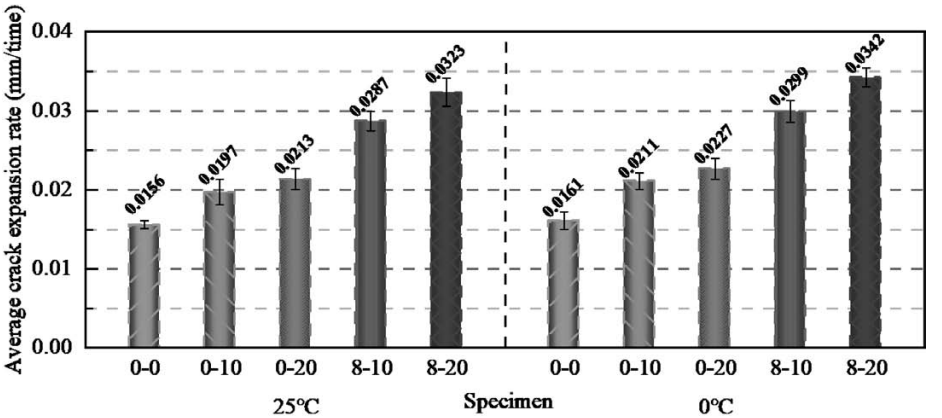

Figure 7: Average crack expansion rate of WRAM under different freeze-thaw cycles

Table 7: Model fitting parameters

Specimen/fitting parameters	v_0	a	b	c	R^2
WRAM	0.016793	-5.1E-05	0.128183	0.000325	0.990

Table 8: Comparison of actual values and fitted values

V/Specimens	25-0-0	25-0-10	25-0-20	25-8-10	25-8-20	0-0-0	0-0-10	0-0-20	0-8-10	0-8-20
Actual values	0.0156	0.0197	0.0213	0.0287	0.0323	0.0161	0.0211	0.0227	0.0299	0.0342
Fitted values	0.0155	0.0188	0.0220	0.0290	0.0323	0.0168	0.0201	0.0233	0.0303	0.0336
Relative errors	0.351%	4.625%	-3.249%	-1.129%	0.161%	-4.242%	4.989%	-2.830%	-1.277%	1.912%

ture conditions, indicating that the salt freeze-thaw cycles had a more significant effect on the anti-reflective cracking ability of WRAM specimens. This is because the WRAM specimens are not only subjected to freezing and erosion damage from water during salt freeze-thaw cycles, but also to the infiltration of de-icing salt, which enters the specimen's tiny pores with the aqueous solution. The salt solution's Na^+, OH^-, and Cl^- ions dissolve the hydrophilic groups in the asphalt. The higher the mass fraction of the salt solution, the more pronounced is the chemical erosion effect. The salt solution generates both swelling and crystallization pressures during the freeze-thaw cycle compared to clear water, resulting in a greater degree of damage to the internal structure of a specimen, which in turn seriously affects the anti-reflective cracking ability of the specimen.[32]

By comparing the variations in CPR and V of the WRAM specimens, it was found that the variation rate of CPR fluctuated significantly under different freeze–thaw cycles, and its results showed poor consistency with the actual occurrence of reflective cracking in the specimens. In contrast, the variation rate of V exhibited a more consistent and predictable trend. Therefore, by employing the digital image correlation (DIC) technology to obtain crack images of WRAM specimens at the end of the test, and calculating the average crack propagation rate based on the measured crack length (L), the index V provides a more direct reflection of the overall time-dependent crack propagation behavior during loading. Compared to CPR, V offers a more stable characterization of the reflective cracking resistance of WRAM specimens. Particularly when the CRR value fluctuates significantly, the V index demonstrates greater representativeness in evaluating the overall crack resistance performance.

3.2 Establishment of the WRAM reflection cracking model

Figure 7 shows that different temperatures and freeze-thaw cycling conditions significantly affect V of the WRAM specimens. There is a correlation between the variation in V and temperature and freeze-thaw cycling conditions. Based on these factors, the functional relationship was determined using the SPSS regression analysis, as shown in Equation 3. The fitting results are shown in **Tables 7** and **8**.

$$V = v_0 + ax + by + cz \tag{3}$$

Here, V is the average crack expansion rate; x is the test temperature; y is the salt solution concentration; z is the number of freeze-thaw cycles; v_0, a, b, c are the fitting parameters.

Tables 7 and **8** show that the relative error between the actual and fitted values is within plus or minus 5 %. There is a polynomial relationship between V and three factors: temperature, salt solution concentration, and the number of freeze-thaw cycles. The fitted correlation (R^2) is 0.99, indicating that the polynomial can effectively predict the anti-reflective cracking characteristics of WRAM under the coupling action of temperature and freeze-thaw cycle. Meanwhile, it is feasible to use DIC to obtain crack images of the specimens at the end of the test and calculate their V values to analyze the anti-reflective cracking ability of WRAM. Therefore, V is recommended as a parameter to further characterize the reflection cracking properties of asphalt mortars under freeze-thaw cycles.

3.3 Analysis of strain distribution in the reflection fracture damaged area

During the loading process, a WRAM specimen exhibits irregular cracks along the center on the left and right sides. DIC is used to capture information before and after the deformation of the specimen's scattered speckles. If only the strain value at a certain point is selected to study the cracking damage of the specimen, there are certain limitations. Therefore, the damaged area must completely cover the crack extension path. At the same time, strain values at multiple points should be selected for the study. Based on the above factors, it is found that a rectangular area of (38 × 20) mm can cover the cracks generated on the entire specimen. **Figure 8** shows cloud maps of vertical strain (*Eyy*) characteristics of the damaged area of a WRAM specimen. Positive values in the graph indicate that the specimen is subjected to tensile stress in the vertical direction; Negative values indicate the action of compressive stress in the vertical direction.

As shown in **Figure 8**, in the initial stage, the bottom of the specimen is in tension under repeated loading, and the strain between the two metal bottom plates appears to be concentrated, but not significant. In the crack forma-

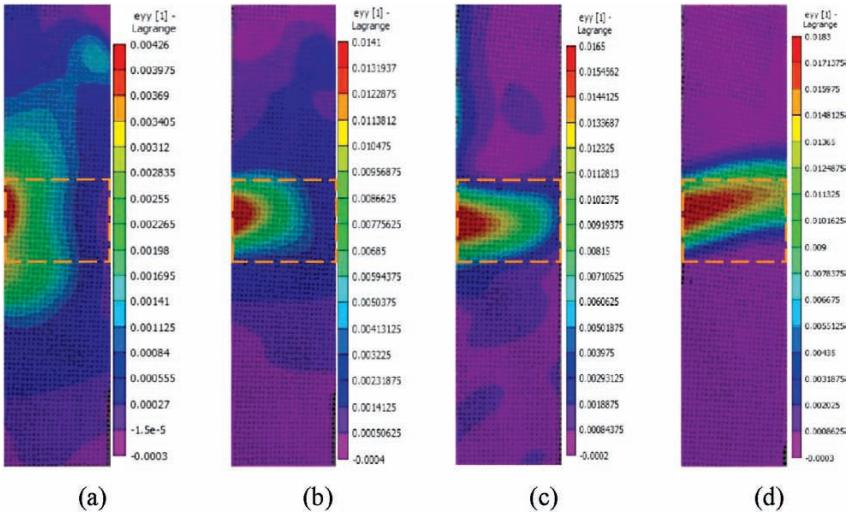

Figure 8: *Eyy* feature cloud map: a) initial; b) formation of cracks; c) development of cracks; d) failure

tion stage, the strain concentration is more significant, and microcracks start to form in the strain concentration area. In the crack development stage, the strain concentration area is further expanded and the microcracks are gradually expanded into reflection cracks. In the failure stage, the strain concentration phenomenon covers almost the entire damaged area; the specimen can no longer withstand the tensile stress, and eventually, failure occurs.

3.4 Effect of freeze-thaw cycling on reflection cracking damage characteristics

Figure 9: Schematic diagram of *Eyy* variation curve

Figure 9 shows the damage region's vertical strain-cycle number (*Eyy-N*) variation curves. As seen in the figure, the *Eyy-N* curve of a WRAM specimen shows a trend of increasing to a peak and then gradually decreasing. This is due to the presence of microcracks and micropores within the WRAM. During the damage accumulation phase, under constant displacement, the internal damage deformation of the specimen results in an accumulation phenomenon, causing the *Eyy* value to show an increasing trend. In the crack propagation phase, when the damage accumulates to a certain extent, macroscopic cracks begin to appear in the specimen, and these cracks gradually expand. At this point, the energy accumulated in the local defect regions of the specimen is released and transferred to other areas, resulting in a peak in the *Eyy* value.

In the energy dissipation and stabilization phase, the energy release and transfer after crack propagation lead to a reestablishment of a relatively stable energy dissipation state within the specimen. At this stage, the *Eyy* value of the specimen gradually decreases and tends toward stability. Therefore, to further analyze the reflective cracking characteristics of WRAM under different freeze-thaw cycles, the cracking damage factor (D_A) can be introduced to characterize the damage development inside the WRAM specimens from the damage accumulation perspective. The specific calculation is shown in **Equations 4** and **5**.

$$D(\varepsilon) = \sum_{1}^{i} Eyy_i \tag{4}$$

$$D_{\mathrm{A}} = \frac{D(\varepsilon)}{D_{\max}} \tag{5}$$

Here, D_{A} is the cracking damage factor; $\sum_{1}^{i} Eyy_i$ is the accumulated value of vertical strain for the i times; $D_{\max}$ is the maximum cumulative value of $D(\varepsilon)$, which is the cumulative value of *Eyy* at the end of the test.

Figure 10 shows the damage factor-cycle number (D_{A}-*N*) variation curve corresponding to the damage area's vertical strain-cycle number (*Eyy-N*) curve. It can be seen that the curve reflects the damage evolution process of the WRAM specimens under different freeze-thaw cycles. Most specimens show a two-stage trend, whereas some curves show a three-stage trend. In the first stage, as the number of cycles increases, the D_{A}-*N* curve of a WRAM specimen grows more slowly, and the rate of damage accumulation is relatively low, showing a better anti-reflective cracking ability. This is because, in the initial stage, the internal structure of the WRAM specimen is relatively uniform and dense, and its ability to bear the load is stronger; hence, the specimen has strong resistance to deformation at this stage.

In the second stage, with the increasing number of load cycles, the rate of damage accumulation of WRAM specimens increases. This is due to the gradual stripping of the asphalt from the fine aggregate interface during the loading of the WRAM specimen, resulting in microcracks on the specimen surface; when the microcracks accumulate to a certain extent, they gradually expand and form macroscopic cracks, thus increasing the rate of curve growth. The D_{A}-*N* curves of 8–20 at 25 °C, and 8–10 and 8–20 WRAM specimens at 0 °C show the third

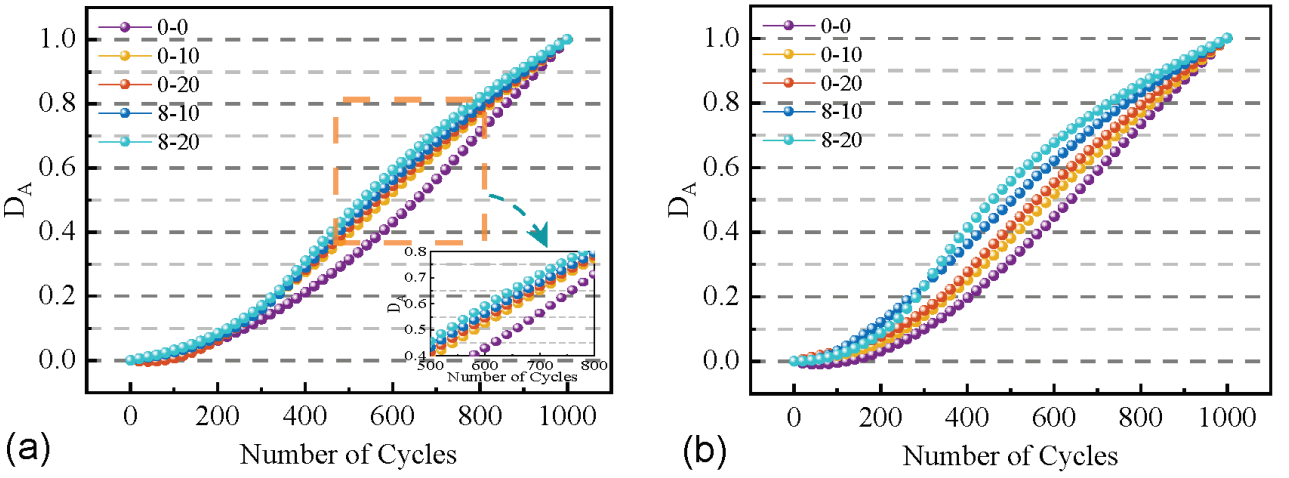

Figure 10: Variation curves in WRAM damage factor D_A under different freeze-thaw cycles: a) 25 °C, b) 0 °C

stage of the variation trend. This is because, in the second stage of a specimen's failure, the reflection crack continues to spread upward as damage accumulates. By the end of the second stage, the crack completely penetrates the entire specimen. At this time, the strength of the specimen is deficient, the strain generated by the specimen is low, and eventually, the D_A-N curve changes.

Secondly, at both 25 °C or 0 °C, with a certain concentration of the salt solution, compared with the original specimen, the slope of the D_A-N curve of a WRAM specimen gradually increases as the number of freeze-thaw cycles increases, and the position of the curve shifts upward, indicating that the anti-reflective cracking ability of the WRAM specimen gradually decreases with the increase in the number of freeze-thaw cycles. This is because water molecules progressively infiltrate the WRAM specimen's pores during the freeze-thaw processes. At low temperatures, the specimen is continuously subjected to frozen swelling caused by the condensation of water into ice. Repeated freezing and swelling forces cause microcracks to form in the specimen, ultimately intensifying the accumulation rate of freeze-thaw damage inside the specimen. In addition, due to the large surface free energy of water, the water continues to diffuse into the fine aggregate surface, resulting in oil and stone debonding, thereby weakening the anti-reflective cracking ability of the specimen.

On the other hand, compared with the original specimens, at both 25 °C and 0 °C, the slope of the D_A-N curve of the WRAM specimens also shows an increasing trend with the increase in the salt solution concentration under a certain number of freeze-thaw cycles. The position of the D_A-N curve is relatively downward after the action of clear-water freeze-thaw cycles. However, after salt freeze-thaw cycles, the slope of the curve increases rapidly, the curve rises upwards, and the anti-reflective cracking ability decreases. This indicates that the anti-reflective cracking ability of the WRAM specimens gradually decreases with increasing salt solution concentration. The effect of salt freeze-thaw cycles on the reflection cracking characteristics of WRAM specimens is more significant than that of clear-water freeze-thaw cycles. This is because the internal voids of the WRAM specimens are gradually enlarged due to repeated freezing and swelling forces, the structure of the specimens is damaged, and the salt solution continuously penetrates the asphalt film, weakening the bonding between the asphalt film and the fine aggregates. Concurrently, the joint action of the freezing and swelling forces of the water and the erosion of de-icing salts exacerbates the rate of damage accumulation within a specimen.

4 CONCLUSIONS

In this study, using macroscopic and mesoscopic methods, we evaluated the anti-reflective cracking ability of warm-mix recycled asphalt mortar (WRAM) under freeze-thaw cycles; the conclusions are as follows:

1) Through the analysis of CPR, it is found that under the same temperature and salt solution concentration, the CPR of WRAM specimens shows an increasing trend with the increase in freeze-thaw cycles. However, there are limitations to using CPR to study the reflection cracking characteristics of WRAM under different freeze-thaw cycles;
2) The V values calculated from crack images can accurately describe the actual cracking of the reflected cracks in the WRAM specimens. V shows an increasing trend with the increase in freeze-thaw cycles. Salt-water freeze-thaw has a more significant effect on V than clear-water freeze-thaw. A decrease in the temperature increases V. At the same time, there is a good correlation between V and the following three factors: temperature, salt solution concentration, and number of freeze-thaw cycles;
3) The cracking damage factor D_A, as defined by Eyy, accurately reflects the reflection cracking characteristics of WRAM under the effect of freeze-thaw cycles.

The D_A-N curve for most WRAM specimens shows a two-stage variation, whereas the D_A-N curve for the specimens under a stronger freeze-thaw cycle shows a three-stage variation. Clear-water freeze-thaw cycles and salt-water freeze-thaw cycles under the same temperature exacerbate the growth rate of the D_A-N curve. The average crack expansion rate V and the cracking damage factor D_A are recommended to be used for evaluating the reflection cracking characteristics of asphalt mortars under freeze-thaw cycles.

Acknowledgments

This work was funded by the National Natural Science Foundation of China Project (No.12262030), the Inner Mongolia Science and Technology Program Project (No.2020GG0263), the Basic Scientific Research Expenses Program of Universities Directly under Inner Mongolia Autonomous Region (No.JY20220005, No.JY20220091), and the Inner Mongolia Autonomous Region Universities Youth Science and Technology Talent Project (No.NJYT22079). The project was also supported by the Open Fund of National Engineering Research Center of Highway Maintenance Technology (Changsha University of Science & Technology) (No.kfj210106) and the Basic Scientific Research Expenses Program of Universities Directly under Inner Mongolia Autonomous Region (No.ZTY2023059).

Author contributions

Jian Gao: Writing–re–view & editing, Supervision. Zhiqiang Liu: Conceptualization, Methodology, Software, Writing–original draft. Chao Li: Funding acquisition, Supervision, Writing–re–view & editing. Lan Wang and Yudong Ma: Formal analysis, Visualization.

Declaration of competing interest

The authors do not have any conflict of interest with other entities or researchers.

5 REFERENCES

[1] L. Jiao, M. Elkashef, J. T. Harvey, M. A. Rahman, D. Jones, Investigation of fatigue performance of asphalt mixtures and FAM mixes with high recycled asphalt material contents, Constr. Build. Mater., 314 (**2022**), 125607

[2] C. Yang, J. Zhang, F. Yang, M. Cheng, Y. Wang, S. Amirkhanian, S. Wu, M. Wei, J. Xie, Multi-scale performance evaluation and correlation analysis of blended asphalt and recycled asphalt mixtures incorporating high RAP content, J. Clean. Prod., 317 (**2021**), 128278

[3] A. A. Yousefi, S. Sobhi, M. R. M. Aliha, S. Pirmohammad, H. F. Haghshenas, Cracking Properties of Warm Mix Asphalts Containing Reclaimed Asphalt Pavement and Recycling Agents under Different Loading Modes, Constr. Build. Mater., 300 (**2021**), 124130

[4] A. Yousefi, A. Behnood, A. Nowruzi, H. Haghshenas, Performance evaluation of asphalt mixtures containing warm mix asphalt (WMA) additives and reclaimed asphalt pavement (RAP), Constr. Build. Mater., 268 (**2021**), 121200

[5] L. P. Ingrassia, F. Cardone, G. Ferrotti, F. Canestrari, Monitoring the evolution of the structural properties of warm recycled pavements with Falling Weight Deflectometer and laboratory tests, Road Mater. Pavement Des., 22 (**2021**), S69–S82

[6] G. Nie, X. Cai, W. Huang, H. M. Z. Hassan, S. Chen, Q. Zhang, J. Xie, K. Wu, Designing of an anti-rutting and High Ductility Asphalt Mixture based on mortar performance, Constr. Build. Mater., 316 (**2022**), 125837

[7] X. Wang, Y. Zhong, Reflective crack in semi-rigid base asphalt pavement under temperature-traffic coupled dynamics using XFEM, Constr. Build. Mater., 214 (**2019**) 280–289

[8] H. Cao, T. Chen, H. Zhu, H. Ren, Influence of Frequent Freeze–Thaw Cycles on Performance of Asphalt Pavement in High-Cold and High-Altitude Areas, Coatings, 12 (**2022**) 6, 752

[9] R. Zhai, P. Hao, G. Li, Z. Zeng, W. Li, Anti-reflection Cracking Performance of Asphalt Mixture under Freeze-Thaw Cycles, J. Build. Mater., 21 (**2018**) 6, 1000–1004

[10] R. Bandaru, Cost Effective Prevention of Reflective Cracking in Composite Pavements, Louisiana State University and Agricultural & Mechanical College, 2010

[11] Q. Fu, J. Wei, L. Wang, Research on Anti-reflective Cracking Performance of Open-graded Large Stone Asphalt Mixes Based on MMLS3, China J. Highw. Transp., 33 (**2020**) 8, 133–143

[12] F. Hou, T. Li, X. Li, Y. Li, M. Guo, Research on the Anti-Reflective Cracking Performance of a Full-Depth Asphalt Pavement, Sustainability, 13 (**2021**) 17, 9499

[13] R. Li, M. Liu, G. Zhou, H. Wang, Z. Zhang, Performance Study of Reflective Resistance Crack of DZFH Road Crack Paste, J. Chongqing Jiaotong Univ. Sci., 36 (**2017**) 10, 51–55

[14] J. Ling, F. Wei, J. Gao, J. Zhang, Y. Tian, Y. Li, New Test Method for Measuring Reflective Cracking in Hot-Mix Asphalt Overlay Pavements, Transp. Res. Rec., 2673 (**2019**) 6, 327–336

[15] B. Yu, Q. Lu, J. Yang, Evaluation of anti-reflective cracking measures by laboratory test, Int. J. Pavement Eng., 14 (**2013**) 6, 553–560

[16] H. Zhang, P. Hao, C. Tang, Y. Pang, Adherence of Geotextile Interlayer in Asphalt Overlay, J. Build. Mater., 20 (**2017**) 5, 745–751

[17] F. Zhou, S. Im, L. Sun, T. Scullion, Development of an IDEAL cracking test for asphalt mix design and QC/QA, Road Mater. Pavement Des., 18 (**2017**) sup4, 405–427

[18] W. Wang, S. Zhou, Yu Qin, Research progress of indoor reflective crack test method, Mater. Rep., 36 (**2022**) 5, 79–88

[19] L. F. Walubita, A. N. M. Faruk, A. E. Alvarez, T. Scullion, The Overlay Tester (OT): Using the Fracture Energy Index concept to analyze the OT monotonic loading test data, Constr. Build. Mater., 40 (**2013**), 802–811

[20] L. F. Walubita, A. N. M. Faruk, J. Zhang, X. Hu, Characterizing the cracking and fracture properties of geosynthetic interlayer reinforced HMA samples using the Overlay Tester (OT), Constr. Build. Mater., 93 (**2015**), 695–702

[21] L. F. Walubita, L. Fuentes, S. I. Lee, O. Guerrero, E. Mahmoud, B. Naik, G. S. Simate, Correlations and preliminary validation of the laboratory monotonic overlay test (OT) data to reflective cracking performance of in-service field highway sections, Constr. Build. Mater., 267 (**2021**), 121029

[22] T. M. Phan, S. N. Nguyen, C.-B. Seo, D.-W. Park, Effect of treated fibers on performance of asphalt mixture, Constr. Build. Mater., 274 (**2021**), 122051

[23] Research institute of highway ministry of transport of the People's Republic of China, JTG F40-2004 Technical specifications for construction of highway asphalt pavements, 2004

[24] J. Hu, L. Wang, C. Guo, H. Liu, Quantitative study on fatigue characteristics of warm mix recycled asphalt, Constr. Build. Mater., 431 (**2024**), 136532

[25] C Li, Z Tian, L Wang, J. Gao, X. Xie, Y. Guo, Evaluation of Anti Reflective Cracking Performance of Warm Mix Recycled Asphalt Mor-

tar Before and After Secondary Aging, J. Munic. Technol., 42 (**2024**) 9, 183–190

[26] Kai Cui, Research on fatigue damage of asphalt mortar, Master's Degree, Southeast University, 2017

[27] Zheng Chen, Research on high temperature performance of composite rubber powder modified asphalt mixture under aging and freezing-thawing conditions, Master's Degree, Inner Mongolia University of Technology, 2021

[28] X. Luo, Study on the effect of freeze-thaw cycle on cracking characteristics of warm mixed rubber powder modified asphalt mixture under fatigue load, Master's Degree, Inner Mongolia University of Technology, 2019

[29] B. Zhang, Experimental study on high and low temperature performance of warm crumb rubber modified asphalt mixtures under freeze-thaw cycle, Master's Degree, Inner Mongolia University of Technology, 2018

[30] V. Garcia, A. Miramontes, J. Garibay, I. Abdallah, S. Nazarian, Improved Overlay Tester for Fatigue Cracking Resistance of Asphalt Mixtures, Center for Transportation Infrastructure Systems, 2017

[31] Z. Guo, L. Wang, L. Feng, Y. Guo, Research on fatigue performance of composite crumb rubber modified asphalt mixture under freeze thaw cycles, Constr. Build. Mater., 323 (**2022**), 126603

[32] J. Wu, T. Zhang, F. Li, Salt-Freezing Damage Performance of Coal Gangue Powder/Polyester Fiber Asphalt Mixture, J. Build. Mater., 25 (**2022**) 5, 516–524